# Energy efficient design of multi-point trajectories for Cartesian robots

Paolo Boscariol and Dario Richiedei

DTG, Università degli Studi di Padova Stradella S. Nicola 3, 36100 Vicenza, Italy
✉ paolo.boscariol@unipd.it

**Abstract**

This paper describes a method for planning energy efficient trajectories for industrial robots driven by brushless or DC motors with regenerative braking. The optimization problem is defined upon spline interpolation methods, using piecewise polynomial functions to produce a trajectory passing trough a sequence of via-points, and on the electromechanical model of the robot. The formulation introduced in this work is aimed at estimating and optimizing the energy consumption using closed-form expressions and therefore without the need for any numerical integration of the robot dynamics. The method accounts for kinematic constraints on speed, acceleration and jerk, as well as constraints due to the limitations of the power supply and of the regenerated energy storage system.

## 1 Introduction

The use of robotic manipulators for the automatic production and handling of goods is experiencing a constant growth. Robots allow to achieve fast and precise operations while lowering the production costs and reducing the exposure of operators to tedious and potentially dangerous tasks.

Since a significant part of the manufacturing cost is due to the price of the energy used during the manufacturing phase, any improvement in this area might be beneficial. The focus on such target is testified both by a flourishing scientific literature, both by the politics set by the European Union policy [1], according to which a reduction of the energy consumption of 30% by 2030 is targeted.n

The manufacturing sector is actually responsible for a significant percentage of the total energetic demand [2], and in this area robotic manipulators and automatic machine plays an essential role [3, 4]. For this reasons the use of technologies and strategies for the optimization of the energetic costs of robots is of paramount importance. It is indeed true that a coordinated and synergistic application of energy-saving methods to key aspects of the whole production process, thus including robot operation, machining [5, 6] and material handling [7] is certainly one of the most promising tool for achieving a truly efficient manufacturing industry.

Focusing just on robots, the work [8] showcases the application of several strategies for achieving power savings up to 40%, by adopting smart solutions for motion planning, energy sharing and intelligent brake managing. The proposed solutions are actually feasible in industrial applications, since virtually all automation components catalog offer energy efficient solutions, such as motor drives with regenerative braking, bi-directional motor drives or energy sharing along DC buses [9, 10].

Such off-the-shelves technological advancements call for the development of novel robot applications specifically aimed at improving the energetic efficiency: in this regard a crucial role is played by trajectory planning algorithms [11]. The choice of motion planning as a fundamental

This is a pre-print of an article published in The International Journal of Advanced Manufacturing Technology.
The final authenticated version is available online at: https://doi.org/10.1007/s00170-018-03234-4

tool for achieving the energy efficient operation of an industrial robot is testified also by the availability of recently approved patents [12, 13]. This fact also showcases the interest on the topic by robot practitioners and manufacturers as well.

The recent literature review [11] collects the main result of a recently flourishing scientific literature on the topic. The impact of the choice of the trajectory operated by and industrial machine has been investigated since the late Seventies, as in the work [14], in which an analytic framework is proposed to evaluate the total energy consumption when DC motors are used. Further developments of the same technique, which uses a simple analytic formulation, can be found in [15] and [16]. The works [15, 16, 17] investigate the design of energy-efficient motion profiles for constant inertia single degree-of-freedom systems. The last one is of particular interest since it proposed a method that enables the analytical computation of the optimal trajectory, therefore it does not require to use numerical integrations or iterative optimization procedures.

A common tool for the computation of optimal motion profiles is the calculus of variation, and in particular the solution of Euler equations, as used in [18, 19]. Calculus of variation is a very elegant and efficient method, especially when an analytical solution can be found. When the latter is not available, the only practical solution is to resort to numerical solutions, which, unfortunately, are generally restricted to problems described by a limited number of state variables [20]. It should be however highlighted that variational formulation used in [18, 19] is limited in generality, given that not all motion design problems can be casted according to the formulation proposed in such works. A common shortcomings of variational problems is also the limited capability in handling dynamics with hard nonlinearities and discontinuities.

An alternative powerful and commonly used tool for computing perfected motion profiles is the use of indirect approaches. The methods belonging to this class are based on the transcription of the original planning problem into a parameter optimization one. Some of such approaches [21, 22] are based on experimentally defined models of the energy flow in multi-axis servo systems and in energy storage devices, while others are based on much more detailed models or virtual prototypes, such as in [23, 24].

The work [21] explores the concept of synchronizing the point-to-point motion of multiple independent axes together with extended DC-link capacitance or flywheels, using an iterative optimization routine. The results are then extended in [22] with further experimental validations. The procedure used in these two works had already been established in [25], in which Hansen et.al. proposed a method to optimize the energy consumption of a 6 dofs industrial robot using iterative numerical integration and limiting to the case of point-to-point motion.

The energy optimization of the motion profile for a slider-crank mechanism is presented in [24]. This work includes a very detailed analytical model of all the mechanical and electrical components of the system. Optimization of the point-to-point motion profile is carried out using the Sequential Quadratic Programming method, by running a MATLAB-Simulink model at each iteration of the optimization routine. A similar problem is investigated also in [23], by substituting the analytical formulations of the dynamic model with look-up tables data obtained from a CAD-bases multibody analysis tool. These works suggest that when the complexity of the model is made high to include a large amount of details and energy dissipation phenomena, or simply machines with a complex dynamics are considered, the use of dynamic simulation provided by dedicated software packages is inevitable. Incorporating into an optimization procedure the results of complex dynamic simulations has the side effect of shifting the balance between accuracy and computational burden towards more computationally demanding solutions.

The aim of this work is to propose an effective and computationally efficient method for the design of minimum energy trajectories for robots with kinematically decoupled axes. An indirect approach is used, since the trajectory for each joint of the robot is defined by spline functions, which can be described by a limited set of parameters. Such parameters can be used to provide an analytic evaluation of the energetic cost associated with the motion design, so that the procedure can be completed without resorting to iterative numerical integrations of the dynamic model of the robot. The choice of suitable spline interpolating functions offers also the possibility of constraining joint speed, acceleration and jerk, as well as to choose the desired level of smoothness by selecting the most suitable motion primitives. The results are then extended to introduce also

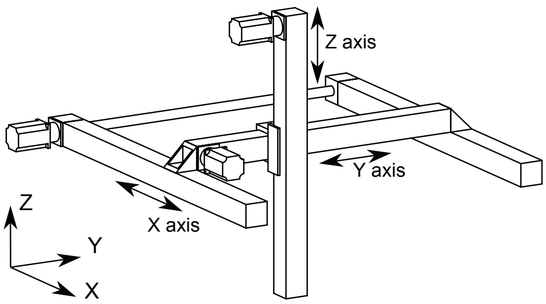


Figure 1: Three axes Cartesian robot

motor current or motor torque limitations for maximum compatibility with industrial applications.

# 2 Energy consumption estimation

In this section the analytical model used for estimating the energy consumption of a multi-axis robot driven by DC or brushless motors and will be recalled. The theory is developed with reference to a three axes Cartesian robot, as the one shown in Fig. 1.

Since each joint of the robot is kinematically and dynamically independent from the others, its dynamic model can be expressed as:

$$J\ddot{q}(t) + T_f(t) + T_c(t) + T_{ext} = \tau_m(t) \tag{1}$$

in which $q(t)$ is the angular position of the motor shaft and $\tau_m(t)$ is the torque exerted by the motor. The moment of inertia $J$ accounts for the contribution of the motor shaft, of the translating load mass and of the transmission as well. $T_f(t) = f_v\dot{q}(t)$ is the viscous friction force (with $f_v$ the viscous coefficient) and $T_c(t) = T_c\, sgn(\dot{q}(t))$ is the Coulomb friction force. External forces, such as the gravity force, can be included in the contribution $T_{ext}$. The motor torque is proportional to the current $I(t)$ drawn by the motor, as:

$$\tau_m(t) = k_t I(t) \tag{2}$$

being $k_t$ the motor torque constant. The voltage drop across the motor is described by:

$$V(t) = RI(t) + k_b\dot{q}(t) + L\frac{dI(t)}{dt} \tag{3}$$

in which $R$ and $L$ are the resistance and the inductance, respectively, of the motor windings and $k_b$ is the motor back-emf constant. The instantaneous electric power drawn by the motor can therefore be estimated as the voltage-current product:

$$W_e(t) = V(t)I(t) \tag{4}$$

The total energy consumption over a time interval $[t_a, t_b]$ can be estimated from the time integral of the electric power $W_e(t)$:

$$E = \eta_d \int_{t_a}^{t_b} W_e(t)dt = \eta_d \int_{t_a}^{t_b} V(t)I(t)dt \tag{5}$$

The overall energy required to operate of the robot, as specified in Eq. 5, is affected by the efficiency of the drive circuit $\eta_d$, according to the approach already used in other works such as [17]. Assuming that the power dissipated by the drive circuit is proportional to the power absorbed by the electric motor, a constant coefficient is sufficient to describe most practical situations [26].

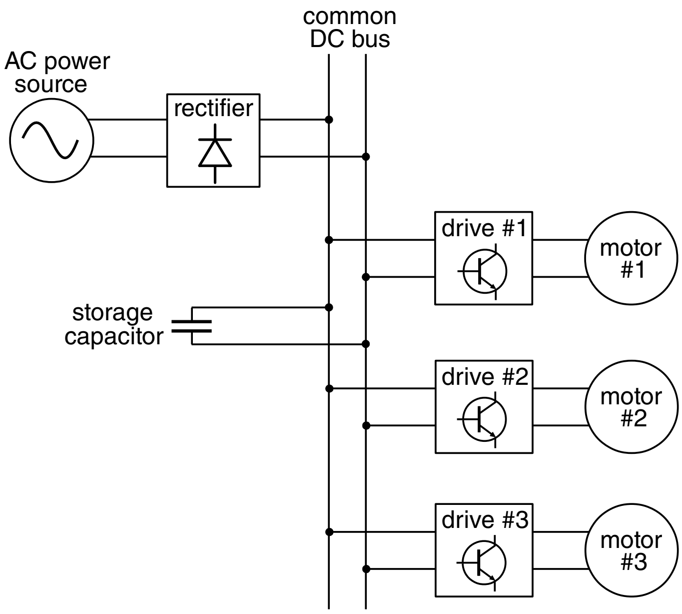


Figure 2: Electric drive: common DC bus connection, with storage capacitor

Without loss of generality, here an unitary drive efficiency is assumed, with the aim of enhancing the readability of the analytical developments that appear in the following sections of this work.

Despite its conceptual simplicity, this model has been used in many works, such as [27, 28], and its capability of faithfully predicting the energy consumption of an industrial application have been reported in [15]. The formulation has been experimentally validated for DC motors [14, 29], for induction motors [30, 19] and for industrial servo systems [21, 25, 31]. It should be noticed that the voltage-to-current product can have also negative values: in this case the electric power will flow from the motor to the electric drive, and therefore a regeneration will take place. In Eq. 5 it is implicitly assumed that all the regenerated energy can be stored by a capacitor or used by other drives connected on the same electric bus, as shown in Fig. 2. This assumption does not limit the validity of the model, since the eventual limitation of the regenerated current can be dealt within the trajectory synthesis phase, as will be shown in the following section. Anyway, it should be noticed that modern industrial applications have the availability of high energy storage capacity, either in the form of extended DC-link capacitance [32], supercapacitors or of additional mechanical axes, e.g. flywheels [22]. Under this assumptions, the overall energy absorbed by the robot is computed as the sum of the energy required by each motor.

It should be highlighted that the formulation of the total energy consumption according to Eq. 1-5 can be used to describe the dynamics of a robot through N independent equations only if the robot axes are kinematically and dynamically decoupled, i.e. if the motion of each axis of the robot is not affected by the motion of the other ones. This feature limits to a reasonable amount the complexity of a closed-form analytic representation of the energy required to perform a trajectory, but the same cannot be stated for a generic robotic architecture in which no mechanical decoupling exist. The most straightforward method to account for other architectures, such as an anthropomorphic configuration, would be to numerically solve the inverse dynamics of the robot, to numerically compute the corresponding values of the instantaneous electric power delivered to each actuator, and to perform a numerical evaluation of the time integral of Eq. 5. This procedure, which has been used, among others, in [25], is more computationally expensive and of lesser flexibility than the analytical closed-form method that is introduced in this paper.

# 3 Spline-based trajectory planning algorithms

In this work four different spline trajectory planning algorithms are taken into consideration, and the analytic formulation of the energy consumption is derived for each of them. The four methods are based a sequence of polynomial functions, defining a trajectory passing trough $N$ via-points, as commonly done for robotic manipulators [33, 34]. These planning methods share the design principle of diving the trajectory into segments, defined by two consecutive via-points: within each segments the motion is described by a polynomial function. The choice of the degree of each polynomial function is usually performed according to the required smoothness. In order to cover a sufficiently wide array of choices, the following algorithms are here adopted: 434 [35], 445 [36], 545 and 5455 [37]. The 434 algorithm uses $4^{th}$-degree polynomials to describe the joint positions for the first segment, i.e between the first and second via-point, and for the last one, while the remaining sections are described by cubic polynomials. Suitable algebraic constraints are imposed to achieve speed and acceleration continuity along the whole motion. If superior smoothness is needed, the 445 trajectory ensures also the jerk continuity for the intermediate via-points, at the cost of generally requiring higher speeds and accelerations [36]. As the name suggests, the first and the intermediate segments are defined as $4^{th}$-degree polynomial functions, while the last segment uses a $5^{th}$-degree polynomial function. Similarly, the 545 trajectory inherits the properties of the 445 trajectory, while adding arbitrary initial jerk for reduced vibration during the initial phases of motion. In order to impose the value of jerk at the final via point as well, the 5455 algorithm can be finally used. This procedure uses quintic splines function for the first, last and next-to-last segments, while the others are based on $4^{th}$-degree ones.

## 3.1 Energy consumption of the 434 trajectory

The formulation of the energy consumption is here analyzed in detail for the 434 trajectory, while for the other three just the final results are given in the Appendix. In order to avoid confusing formulations, all the formulas are reported for a single axis of the robot, since the extension to the multiple axis case is straightforward for kinematically and dynamically independent axes.

### 3.1.1 Trajectory computation

The procedure requires to specify $N$ via-points in the joint space through which the trajectory should pass at some prescribed time instants, collected by vector $\mathbf{Q} = [Q_1, \ldots, Q_N]$, together with the initial and final joint velocities $V_1$ and $V_N$ (which are usually set to zero in a rest-to-rest motion). According to this notation, the joint position during the $k$-th intermediate section, i.e. the one between the consecutive point $Q_k$ and $Q_{k+1}$ (with $2 \leq k \leq N-2$) is described by the cubic polynomial function:

$$q_k(t) = b_{k,1} + b_{k,2}t + b_{k,3}t^2 + b_{k,4}t^3 \tag{6}$$

with $0 \leq t \leq T_k$, in which $T_k$ is the time duration of the $k$-th segment of the trajectory . The values of the four coefficients $b_{k,n}$ are univocally defined through the boundary positions $Q_k$ and $Q_{k+1}$ speeds $V_k$ and $V_{k+1}$ as:

$$\begin{bmatrix} b_{k,1} \\ b_{k,2} \\ b_{k,3} \\ b_{k,4} \end{bmatrix} = \begin{bmatrix} 1 & 0 & 0 & 0 \\ 0 & 1 & 0 & 0 \\ -\dfrac{3}{T_k^2} & -\dfrac{2}{T_k} & \dfrac{3}{T_k^2} & -\dfrac{1}{T_k} \\ \dfrac{2}{T_k^3} & \dfrac{1}{T_k^2} & -\dfrac{2}{T_k^3} & \dfrac{1}{T_k^2} \end{bmatrix} \begin{bmatrix} Q_k \\ V_k \\ Q_{k+1} \\ V_{k+1} \end{bmatrix} \tag{7}$$

The five unknown coefficients $b_{1,n}$ of the first polynomial (i.e. for $k = 1$) are linked to their

This is a pre-print of an article published in The International Journal of Advanced Manufacturing Technology.
The final authenticated version is available online at: https://doi.org/10.1007/s00170-018-03234-4

boundary conditions as follows:

$$\begin{bmatrix} b_{1,1} \\ b_{1,2} \\ b_{1,3} \\ b_{1,4} \\ b_{1,5} \end{bmatrix} = \begin{bmatrix} 1 & 0 & 0 & 0 \\ 0 & 0 & 0 & 0 \\ 0 & 0 & 0 & 0 \\ -\dfrac{4}{T_1^3} & 0 & \dfrac{4}{T_1^3} & -\dfrac{1}{T_2^2} \\ \dfrac{3}{T_1^4} & 0 & -\dfrac{3}{T_1^4} & \dfrac{1}{T_1^3} \end{bmatrix} \begin{bmatrix} Q_1 \\ V_1 \\ Q_2 \\ V_2 \end{bmatrix} \tag{8}$$

The coefficients of the last segment are linked to the boundary conditions at the last and next-to-last via point as specified as follows:

$$\begin{bmatrix} b_{N-1,1} \\ b_{N-1,2} \\ b_{N-1,3} \\ b_{N-1,4} \\ b_{N-1,5} \end{bmatrix} = \begin{bmatrix} 1 & 0 & 0 & 0 \\ 0 & 1 & 0 & 0 \\ -\dfrac{6}{T_{N-1}^2} & -\dfrac{3}{T_{N-1}} & \dfrac{6}{T_{N-1}^2} & 0 \\ \dfrac{8}{T_{N-1}^3} & \dfrac{3}{T_{N-1}^2} & -\dfrac{8}{T_{N-1}^3} & 0 \\ -\dfrac{3}{T_{N-1}^4} & -\dfrac{1}{T_{N-1}^3} & \dfrac{3}{T_{N-1}^4} & 0 \end{bmatrix} \begin{bmatrix} Q_{N-1} \\ V_{N-1} \\ Q_N \\ V_N \end{bmatrix} \tag{9}$$

Computing the polynomial coefficients using Eqs. 7,8 and 9 still requires to evaluate $N-2$ unknown values of speed at via-points, i.e. $V_2, V_3, \ldots, V_{N-2}$. The unknown speeds at intermediate via-points can be found by enforcing the continuity of accelerations at the very same $N-2$ via points, so that:

$$\ddot{q}_k(T_k) = \ddot{q}_{k+1}(0) \tag{10}$$

with $1 \leq k \leq N-2$. The resulting $N-2$ equations can be collected as the linear system of equations:

$$\mathbf{A}\mathbf{d} = \mathbf{h} \tag{11}$$

The column vector $\mathbf{d}$ includes all the unknown velocities at the intermediate via-points:

$$\mathbf{d} = [V_2, V_3, \ldots, V_{N-1}]^T \tag{12}$$

The right-hand side vector in Eq. 11 depends on the known positions $Q_k$ and on the time durations $T_k$:

$$\begin{aligned}
h_1 &= \frac{6}{T_1^2}(Q_2 - Q_1) + \frac{3}{T_2^2}(Q_3 - Q_2) \\
h_2 &= \frac{3}{T_2 T_3}\left[T_2^2(Q_4 - Q_3) + T_3^2(Q_3 - Q_2)\right] \\
&\vdots \\
h_{k-3} &= \frac{3}{T_{k-1}T_k}\left[T_{k-1}^2(Q_k - Q_{k-1}) + T_k^2(Q_{k-1} - Q_{k-2})\right] \quad k = 4, .., N-2 \\
&\vdots \\
h_{N-3} &= \frac{3}{T_{N-3}T_{N-2}}\left[T_{N-3}^2(Q_{N-1} - Q_{N-2}) + T_{N-2}^2(Q_{N-2} - P_{N-3})\right] \\
h_{N-2} &= \frac{3}{T_{N-2}^2}(Q_{N-1} - Q_{N-2}) + \frac{6}{T_{N-1}^2}(Q_N - Q_{N-1})
\end{aligned}$$

Matrix $\mathbf{A}$ is a combination of the time intervals $T_k$. Such a matrix is tridiagonal, and the elements on its main diagonal are:

$$\mathbf{d_A} = \left[\frac{3}{T_1} + \frac{2}{T_2}, 2\left(T_2 + T_3\right), \ldots, 2\left(T_{N-3} + T_{N-2}\right), \frac{2}{T_{N-2}} + \frac{3}{T_{N-1}}\right] \tag{13}$$

while the diagonals above and below the main one are, respectively:

$$\mathbf{d}_{\mathbf{A}+1} = \left[\frac{1}{T_2}, T_3, \ldots, T_{N-2}\right] \tag{14}$$

$$\mathbf{d}_{\mathbf{A}-1} = \left[T_3, \ldots, T_{N-2}, \frac{1}{T_{N-1}}\right] \tag{15}$$

This formulation is chosen since it is computationally efficient, a feature that is needed for large sequences of via-points. Indeed, the matrix inversion that is required to solve Eq. 11 for the velocities can be efficiently computed by Gauss elimination being matrix $\mathbf{A}$ tridiagonal.

The equations above therefore allow to uniquely define a trajectory passing trough all the via-points, for a choice of the $N$ via-points, the initial and final velocities, and the vector of time intervals $\mathbf{T} = [T_1, \ldots, T_{N-1}]$

A similar procedure can be followed to obtain the formulation for the 445 trajectory, which requires the inclusion of jerk continuity conditions at via-points in addition to the continuity conditions of Eq. 10 and to specify initial and final joint acceleration, as specified in [36]. In the case of the 545 and 5455 trajectories the reader can refer to [37].

### 3.1.2 Computation of the energetic cost

The formulation of the electric power of a joint can be written, with reference to the $k$-th segment of the trajectory, according to Eq. 1,2–4 as follows:

$$\begin{aligned} W_{e,k}(t) &= V(t)I(t) = RI^2(t) + k_b I(t)\dot{q}(t) \\ &= W_{Joule,k}(t) + W_{m,k}(t) \end{aligned} \tag{16}$$

Equation 16 highlights that the electric power includes both Joule losses $W_{Joule}$ and the mechanical power $W_m$; the effects of the inductance, which are negligible, are neglected. Joule losses can be written as:

$$W_{Joule,k}(t) = \frac{R}{k_t^2}\left(J\ddot{q}(t) + f_v\dot{q}(t) + T_c\, sgn\left(\dot{q}(t)\right) + T_{ext}\right)^2 \tag{17}$$

or, showing all the terms:

$$\begin{aligned} W_{Joule,k}(t) &= 2\frac{R}{k_t^2}T_c\left(\left(J\ddot{q}(t) + T_{ext}\right) sgn(\dot{q}(t)) + f_v|\dot{q}(t)|\right) \\ &+ \frac{R}{k_t^2}\left(J^2\ddot{q}(t) + {f_v}^2\dot{q}(t)^2 + T_c^2 + T_{ext}^2 + 2Jf_v\dot{q}(t)\ddot{q}(t) + 2JT_{ext}\ddot{q}(t) + 2f_vT_{ext}\dot{q}(t)\right) \end{aligned} \tag{18}$$

The mechanical power is:

$$W_{m,k} = \frac{k_b}{k_t}\left(J\ddot{q}(t) + f_v\dot{q}(t) + T_{ext}\right)\dot{q}(t) + \frac{k_b}{k_t}T_c|\dot{q}(t)| \tag{19}$$

Now the expression of the instantaneous electric power, i.e. the sum of Eq. 18 and Eq. 19, can be re-arranged by separating the terms proportional to $|\dot{q}(t)|$ and to $sgn(\dot{q}(t))$ as:

$$W_{e,k}(t) = W_{1,k}(t) + W_{2,k}(t) + W_{3,k}(t) \tag{20}$$

The proposed re-arrangement allows for a simpler evaluation of both the electric power and the energy consumption in the $k$-th segment of the trajectory. Each term is discussed separately in the following. The terms included in $W_{1,k}$ are a combination of the joint variables $q(t)$, $\dot{q}(t)$, $\ddot{q}(t)$ and of the constant parameters $k_t$, $k_b$, $J$, $T_c$, $T_{ext}$. Since the joint variable are described as time polynomials according to the choice of the motion primitives, the power contributions included in $W_{1,k}(t)$ can be written in a compact polynomial form:

$$W_{1,k}(t) = \sum_{i=0}^{4} w_{i,k}t^i \tag{21}$$

This polynomial form is particularly convenient for the computation of its time integral over the interval $[0, T_k]$, which is:

$$E_{1,k} = \int_0^{T_k} W_{1,k}(t)dt = \sum_{i=0}^{4} \frac{w_{i,k}}{i+1} T_k^{i+1} \tag{22}$$

The expression of the the polynomial coefficients $w_{i,k}$ depend on the specific segment of the trajectory under investigation. For the 434 trajectory, three different formulations must be used for the first segment, for the intermediate ones and the last one. In particular, for the intermediate segments, i.e. for $2 \leq k \leq N-2$, the following holds:

$$w_{4,k} = \frac{9{b_3}^2 f_v \left(R f_v + k_b k_t\right)}{{k_t}^2} \tag{23}$$

$$w_{3,k} = \frac{6 b_3 k_b \left(3 J b_3 + 2 b_2 f_v\right)}{k_t} + \frac{12 R b_3 f_v \left(3 J b_3 + b_2 f_v\right)}{{k_t}^2} \tag{24}$$

$$\begin{aligned} w_{2,k} = & \frac{k_b \left(f {b_2}^2 4 + J b_3 b_2 18 + 3 T_{ext} b_3 + 6 b_1 b_3 f\right)}{k_t} \\ & + \frac{2R \left(18 J^2 {b_3}^2 + 18 J b_2 b_3 f_v + 2 {b_2}^2 f^2 + 3 b_1 b_3 f^2 + 3 T_{ext} b_3 f\right)}{{k_t}^2} \end{aligned} \tag{25}$$

$$\begin{aligned} w_{1,k} = & \frac{2 k_b \left(T_{ext} b_2 + 2 J {b_2}^2 + 3 J b_1 b_3 + 2 b_1 b_2 f\right)}{k_t} \\ & + \frac{4R \left(3 J b_3 + b_2 f\right) \left(T_{ext} + 2 J b_2 + b_1 f\right)}{{k_t}^2} \end{aligned} \tag{26}$$

$$\begin{aligned} w_{0,k} = & \frac{R \left(4 J^2 {b_2}^2 + 4 J T_{ext} b_2 + 4 J b_1 b_2 f_v + {T_c}^2 + {T_{ext}}^2 + 2 T_{ext} b_1 f_v + {b_1}^2 f^2\right)}{{k_t}^2} \\ & + \frac{b_1 k_b \left(T_{ext} + 2 J b_2 + b_1 f\right)}{k_t} \end{aligned} \tag{27}$$

The formulas for $k = 1$ and for $k = N-1$ are reported in Appendix A.

As far as $W_{2,k}$ is concerned, it can be written as:

$$W_{2,k}(t) = 2 \frac{R}{k_t^2} T_c \left(J \ddot{q}(t) + T_{ext}\right) sgn(\dot{q}(t)) \tag{28}$$

It can be noticed that the contribution:

$$2 \frac{R}{k_t^2} J T_c \ddot{q}(t) sgn\left(\dot{q}(t)\right) \tag{29}$$

is relevant in terms of instantaneous power, but its contribution to the overall energy is null, as will be shown here. The contribution can be evaluated for the whole duration of the trajectory, i.e. between 0 and $T$, by splitting the integral into segments delimited by a change of the sign of speed, which happens at time $t_i$ with $i$ ranging from 1 to $m$:

$$\int_0^T \ddot{q}(t)\, sgn\left(\dot{q}(t)\right) dt = \int_0^{t_1} \ddot{q}(t) dt - \int_{t_1}^{t_2} \ddot{q}(t) dt + \ldots \pm \int_{t_m}^{T} \ddot{q}(t) dt \tag{30}$$

Since joint speed is a continuous function, and since the change of sign of speed can happens only when $\dot{q}(t) = 0$, i.e.:

$$\dot{q}(0) = \dot{q}(t_1) = \dot{q}(t_i) = \dot{q}(T) = 0 \tag{31}$$

the time integral of the contribution in Eq. (30) is always zero for a rest-to-rest motion.

The evaluation of the energy consumption associated with the other power term of Eq. 17 requires to find a closed-form expression for the time integral extended to the whole duration of the trajectory:

$$2\frac{R}{k_t^2} T_c T_{ext} \int_0^T sgn(\dot{q}(t))dt \tag{32}$$

Again, making use of the time instants $t_i$ at which $\dot{q}(t) = 0$, i.e. a change of the sign of speed happens, a piecewise integration can be performed, to that:

$$\int_0^T sgn(\dot{q}(t))dt = sgn(\dot{q}(0^+)) \left( \int_0^{t_1} dt - \int_{t_1}^{t_2} dt + \int_{t_2}^{t_3} dt - \ldots \pm \int_{t_m}^{T} dt \right) \tag{33}$$

An equivalent closed-form expression that involves only sums and products is:

$$\int_0^T sgn(\dot{q}(t))dt = sgn(\dot{q}(0^+)) \left( 2\sum_{i=1}^{m} (-1)^{i+1} t_i + (-1)^m T \right) \tag{34}$$

The evaluation of Eq. 34 requires to compute the sign of the joint speed at the beginning of the segment, indicated as $sgn(\dot{q}(0^+))$, which can be simply evaluated as the sign of $\dot{q}(t)$ for a small value of $t$, such as 1 ms. Moreover, the roots of the joint speed, i.e. $t_i$, are needed: their quick computation can be achieved using the matrix companion method [38], and therefore without the need for an iterative method.

The last power term for which a closed-form expression of its time integral is sought is $W_{3,k}$:

$$W_{3,k}(t) = T_c \left( 2\frac{R}{k_t^2} f_v + \frac{k_b}{k_t} \right) |\dot{q}(t)| \tag{35}$$

The correct formula for evaluating the time integral of $|\dot{q}(t)|$ can be found by piecewise integration of $\dot{q}(t)$ within the whole trajectory, by separating the segments over which $\dot{q}(t)$ is either positive or negative:

$$\int_0^T |\dot{q}(t)|dt = sgn\left(\dot{q}(0^+)\right) \cdot \left( (-1)^{i+1} Q_1 + (-1)^i Q_N - 2\sum_{i=1}^{m} (-1)^i q(t_i) \right) \tag{36}$$

Summing all the contributions for a single joint for the whole duration of the trajectory, as provided by Eqs. 22, 28, 34, 35 and 36, the complete formulation of the consumed energy is:

$$\begin{aligned} E = & \sum_{k=1}^{N-1} \left( \sum_{i=0}^{4} \frac{w_{i,k}}{i+1} T_k^{i+1} \right) + \frac{2R}{k_t^2} T_c T_{ext}\, sgn\left(\dot{q}(0^+)\right) \left( 2\sum_{i=1}^{m} (-1)^{i+1} t_i + (-1)^m T \right) \\ & + T_c \left( \frac{2R}{k_t^2} fv + \frac{k_b}{k_t} \right) sgn\left(\dot{q}(0^+)\right) \left( (-1)^{i+1} Q_1 + (-1)^i Q_N - 2\sum_{i=1}^{m} (-1)^i q(t_i) \right) \end{aligned} \tag{37}$$

# 4 Energy optimization

The formulas reported above, and in particular Eq. 37, can be used to formulate an energy optimization problem. The total energy consumption $E$ is parametrized by the vector of time intervals $\mathbf{T} = [T_1, \ldots, T_{N-1}]$ and therefore Eq. 37 can be directly used as the cost function. The following optimization problem is proposed:

$$\begin{cases} \min\limits_{[T_1,..,T_{N-1}]} E_{tot} = \min\limits_{[T_1,..,T_{N-1}]} \sum\limits_{j=1}^{3} \sum\limits_{k=1}^{N-1} E_{k,j} \\ \\ \text{subject to:} \\ \\ V_{min,j} \leq \dot{q}_j(t) \leq V_{max,j}; \\ A_{min,j} \leq \ddot{q}_j(t) \leq A_{max,j}; \\ J_{min,j} \leq \dddot{q}_j(t) \leq J_{max,j}; \\ \\ \text{with: } j = 1, 2, 3;\ k = 1 \ldots N-1; \end{cases} \tag{38}$$

in which $E_{tot}$ is the overall energy consumption of the robot, defined to comply with predefined maximum and minimum values of joint speed, acceleration and jerk, according to the manipulator limitations and to the smoothness requirements. The energy is evaluated by collecting the contribution of the three joints of the robot over $N-1$ segments of the trajectory. The outcome of the optimization problem of Eq. 38 is a vector of optimal sequence of time intervals $\mathbf{T} = [T_1, \ldots, T_{N-1}]$ that ensures minimal overall energy consumption.

The optimization problem is not convex, however a clever selection of the initial guess has shown to be capable of getting rid of this issue and to boost the achievement of significant energy reductions. An initial guess for the choice of the time intervals $T_i$ can be effectively obtained using either the chord length distribution or the centripetal distribution methods, as often proposed in literature [33].

The inclusion of constraints is quite straightforward given that the maximum values of the kinematic quantities are easily parametrized by the time intervals $T_i$, see e.g. [35, 36, 37], and by the suggested parametrization in terms of time intervals $T_i$ of the cost function which is highlighted in Eq. 37.

# 5 Test case I: pick & place task

The dynamic properties of the manipulator used as the test bench for the optimization procedures are listed in Table 1. The same table includes also the maximum values for speed, acceleration and jerk expressed in the operative space. The proposed optimization method is first used to compute

| parameter | joint #1 | joint #2 | joint #3 |
|---|---|---|---|
| Moment of inertia $J$ $[kgm^2]$ | 0.018 | 0.01125 | 0.00675 |
| $f_v$ $[Nm\,s/rad]$ | $5e^{-3}$ | $5e^{-3}$ | $5e^{-3}$ |
| $T_c$ $[Nm]$ | $5e^{-2}$ | $5e^{-2}$ | $5e^{-2}$ |
| $k_t$ $[Nm/A]$ | 0.65 | 0.65 | 0.65 |
| $k_b$ $[V\,s/rad]$ | 0.65 | 0.65 | 0.65 |
| $R$ $[\Omega]$ | 3.3 | 3.3 | 3.3 |
| Max. speed $[m/s]$ | 1.5 | 1.5 | 1.5 |
| Max. acceleration $[m/s^2]$ | 2.5 | 2.5 | 2.5 |
| Max. jerk $[m/s^3]$ | 20 | 20 | 20 |

Table 1: Dynamic properties of the manipulator

the energy-optimal trajectories for the typical pick & place task, which is commonly performed by robot in industry. Such a task is defined by the 9 via-points reported in Table 2.

The end-effector path associated with the energy-optimal solution when choosing the 434 method is shown in Fig. 3.

This is a pre-print of an article published in The International Journal of Advanced Manufacturing Technology.
The final authenticated version is available online at: https://doi.org/10.1007/s00170-018-03234-4

| Via-point | X [mm] | Y [mm] | Z [mm] |
|---|---|---|---|
| 1 | 0 | 0 | 0 |
| 2 | 0 | 0 | 340 |
| 3 | 20 | 25.8 | 380 |
| 4 | 60 | 77.2 | 400 |
| 5 | 250 | 450 | 400 |
| 6 | 640 | 822.8 | 400 |
| 7 | 680 | 874.2 | 380 |
| 8 | 700 | 900 | 340 |
| 9 | 700 | 900 | 0 |

Table 2: Via-points for the pick & place task

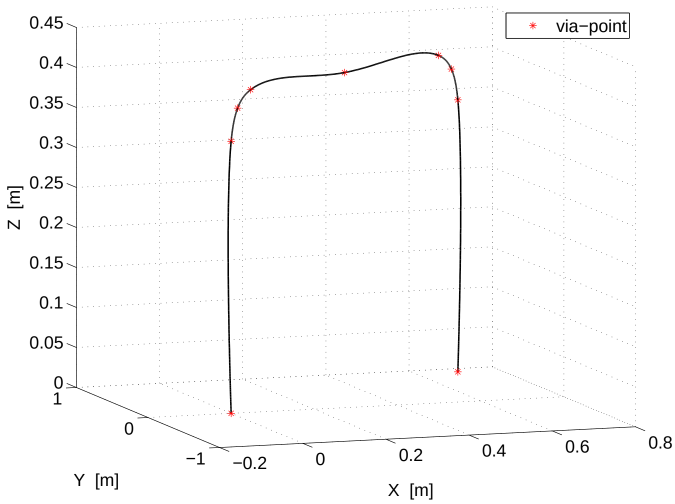


Figure 3: Via-points and end-effector path in the operative space for the pick & place task, with the 434 trajectory

The optimization problem of Eq. 38 can be applied again to the same task with the other three trajectories as well, therefore using the 445, 545 and 5455 methods. In all cases the total execution time is left free, so that the four solution will lead to different total execution times and four different energy requirements. To establish a comparison with other commonly used planning method, the time and energy required in each of the four cases is compared with the results obtained when choosing, instead of the energy-optimal timing of the trajectory, the timing resulting from a chord length distribution and the timing resulting from the minimum time solution. When using the chord length distribution the time required to move between two consecutive via-points is a fraction of the overall motion time, and the ratio between the two is set by the ratio between the chordal distance between the two via-points and the chordal length of the whole path. A proper scaling is then applied when the total execution time that arises from the energy optimal solution is not compatible with the kinematic constraints. In the minimum time solution the trajectory is designed to achieve the absolute minimum time to complete the task while respecting the very same kinematic constraints as in the other two cases. Therefore, whenever made possible by the kinematic constraints, the trajectory designed with the chord length method will have the same duration as the energy optimal one. The overall times and energy consumption resulting from this analysis are reported in Figs. 4 and 5, respectively.

The data presented in Fig. 4 show that the chord length distribution is quite unsuitable to produce fast trajectories, given that the energy-optimal solution results in faster motion in all four cases. The performance degradation is more evident in the cases of 545 and 5455 trajectories, for

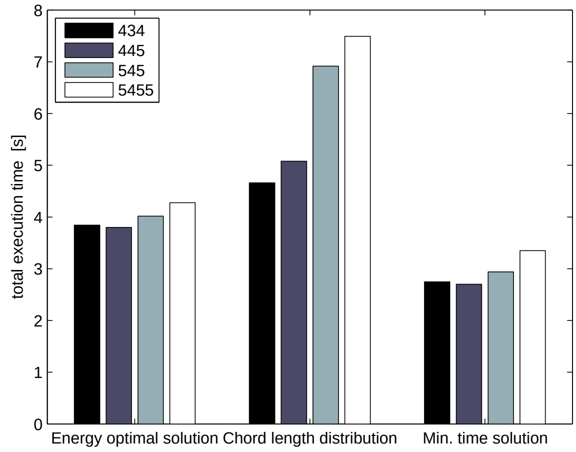


Figure 4: Total execution time for the pick & place task, with the 4 trajectories: comparison between energy-optimal solutions, chord-length time distribution solutions and minimum time solutions

which a heavy time scaling is required to enforce constraints.

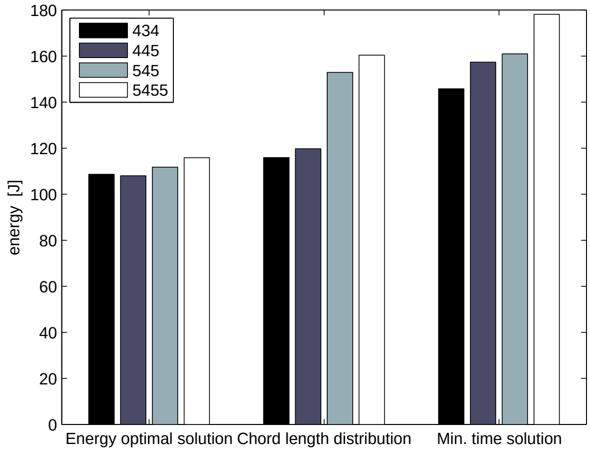


Figure 5: Energy consumption for the pick & place task, with the 4 trajectories: comparison between energy-optimal solutions, chord-length time distribution solutions and minimum time solutions

As far as the energy consumption is taken into consideration, the data shown in Fig. 5 highlight that the use of a trajectory designed by setting the time distance between consecutive via points according to chord length distribution can however lead to results that are quite close to the energy optimality for the two simpler methods, i.e. for the 434 and the 445 trajectories, while a sensible performance degradation is made evident for the two smoother trajectories, i.e. for the 545 and 5455 trajectories. By comparing the energy optimal solutions with the minimum time solutions, therefore looking at the first and last groups of bars in Figs. 4 and 5, it can be noticed that for the case under consideration the proposed solution leads to significant energy improvements at the cost of a significantly slower execution, so in some practical applications it might be desirable to adopt a mixed penalty function that takes into account both design objectives.

This is a pre-print of an article published in The International Journal of Advanced Manufacturing Technology.
The final authenticated version is available online at: https://doi.org/10.1007/s00170-018-03234-4

## 5.1 Energy optimality vs. time

The properties of the four optimal trajectories in terms of electric power is shown in Fig. 6, which plots the time evolution of the electric power absorbed by the actuator which drives the Z axis, and Fig. 7, which shows the overall power absorption by the three actuators when performing the pick & place task already discussed above. In particular, Fig. 6 reveals that, as expected, the motion of the Z axis against gravity during the initial phase of the task is responsible for the largest power usage. During the last phase, which involves the lowering of the Z axis, the power consumption is minimal, since motion happens in the same direction of gravity force. The electric power takes negative values for a brief phase, meaning that some current can be generated and fed back to the electric drive by the Z axis actuator. The amount of regenerated energy is however quite limited, given that the work done by gravity force is mostly compensated by the mechanical and electric losses. A similar situation is found by looking at Fig. 7, which shows the total electric power for the same task and trajectory: even by summing all the contributions of the three actuators, the amount of regenerated energy is still small.

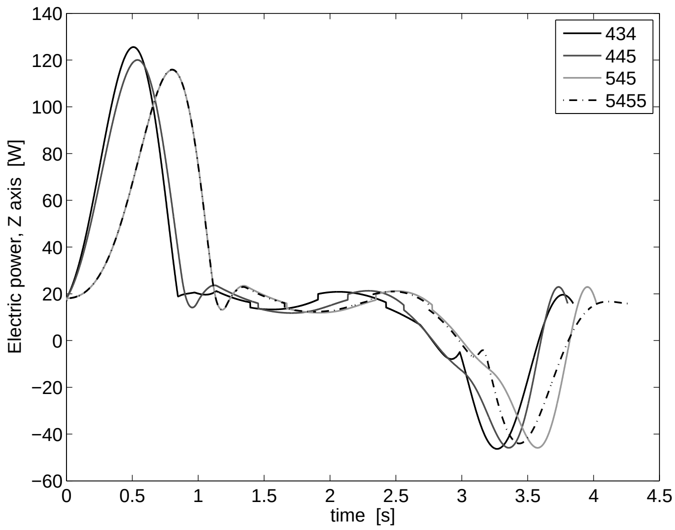


Figure 6: Minimum energy pick & place trajectory: electric power delivered to the motor, Z axis

The motion profiles resulting form the energy-optimal trajectory design for the pick & place task are shown in Figs. 8–10. Such figures present the results just for the Z axis, by plotting the velocity, acceleration and jerk profiles in the operative space according to each of the four algorithms investigated in this work. Figure 8 shows that all the optimal solutions lead to similar maximum speed, and that the energy-optimal trajectories are executed at a speed that is well below the maximum allowed by the kinematic limits. As far as the acceleration along the Z-axis is concerned, all the planning methods, with the exception of the 445 one, require a maximum deceleration that reach the imposed acceleration limit. The slightly improved energetic performance of the 445 planing method over the 434 can be explained by comparing the most significant contribution to the energetic cost, i.e. the power needed to the compensate of the inertial component of motion. The latter can be estimated by the integral of the squared accelerations: according to this metric, the lowest value is found, as expected, for the most efficient trajectory, i.e. the one produced by using the 445 interpolation method. Performing a similar analysis by measuring the total integral of squared jerk shows that the 445 method produces also the smoothest motion. Fig. 10 shows the time evolution of the joint jerk for the Z axis, and highlights the jerk discontinuities sported by the 434 method.

This is a pre-print of an article published in The International Journal of Advanced Manufacturing Technology.
The final authenticated version is available online at: https://doi.org/10.1007/s00170-018-03234-4

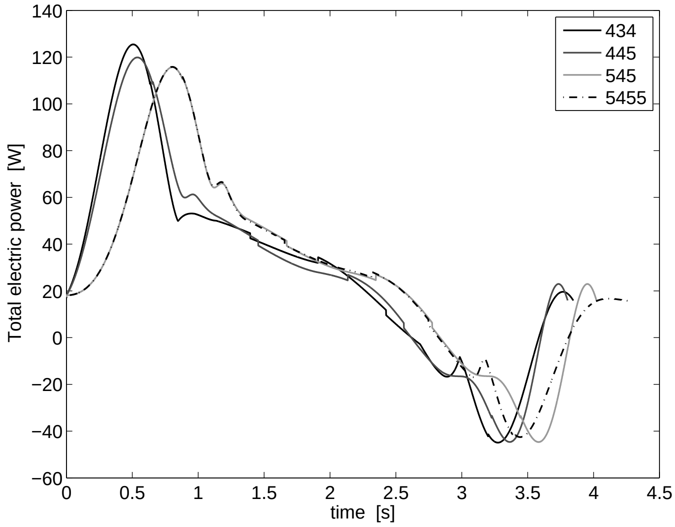


Figure 7: Minimum energy pick & place trajectory: total electric power delivered to the motors

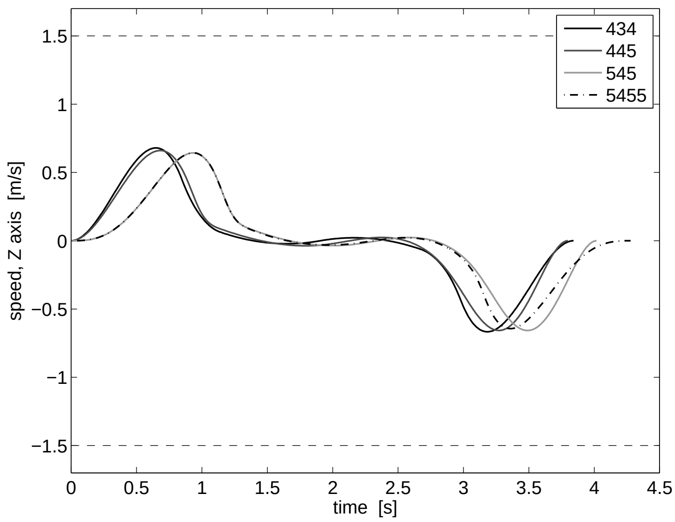


Figure 8: Minimum energy pick & place trajectory: end-effector speed in the operative space, Z axis

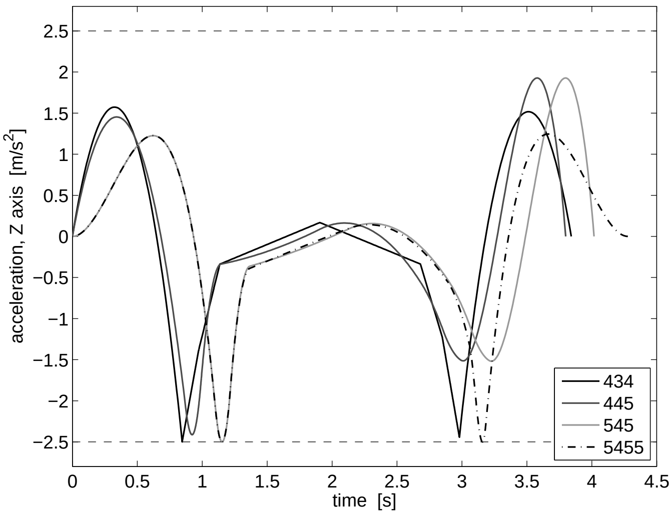


Figure 9: Minimum energy pick & place trajectory: end-effector acceleration in the operative space, Z axis

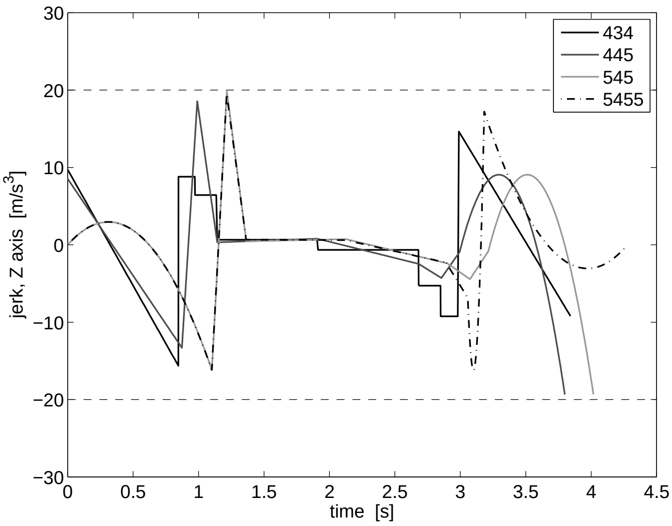


Figure 10: Minimum energy pick & place trajectory: end-effector jerk in the operative space, Z axis

A more general evaluation of the impact of the choice of the trajectory primitive on the overall energy consumption for the pick & place task can be performed by looking at the data provided in Fig. 11. The graph shows the amount of energy required by the robot as a function of the total execution time. The results indicate that the 434 and 445 trajectories lead to very similar energetic requirements, regardless of the overall task duration. Moreover, Fig. 11 also shows that the impact of the choice of the trajectory primitive on the total energy consumption is particularly significant when reduced cycle times are needed, and that such a difference almost vanished as the task duration is increased significantly. This effect can be explained by considering that when the robot is operated at low speed the overall energy consumption is dominated by constant power terms, such as the ones required to counteract gravity or static friction.

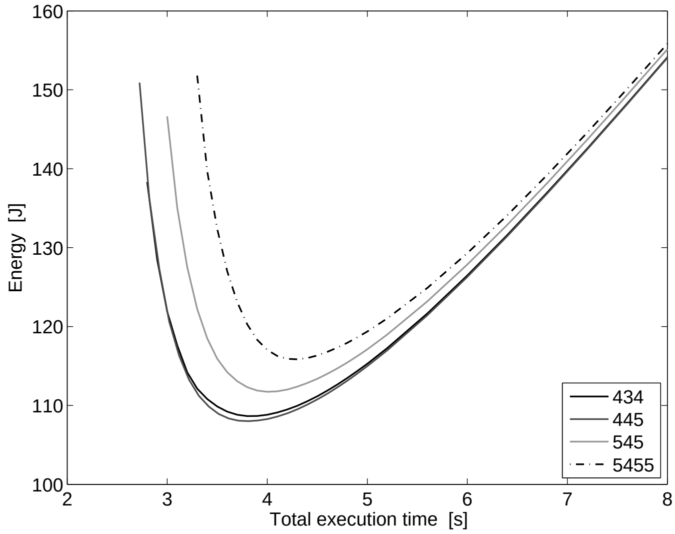


Figure 11: Minimum energy consumption trajectories for the pick & place task: comparison between different planning methods

# 6 Test cases II, III and IV

Three additional tests have been defined to highlight the capability of the proposed method of producing feasible and effective trajectories. Each test is identified by the shape of the sequence of via-points, which are defined in the operational space and reported in Tables 2 and 3–5. Since the four aforementioned planning methods are applied to each task, the additional data can provide some further insight into the choice of the most suitable method.

Task II, referred as "S–shape motion", consists in an open-path motion that involves the simultaneous operation of all the axes of the robot. Tasks III and IV reproduce two slightly more complicated tasks, designed as a sequence of 13 via-points located along a triangular and square profiles, respectively.

| Via-point | X [mm] | Y [mm] | Z [mm] |
|---|---|---|---|
| 1 | 0 | 0 | 200 |
| 2 | 100 | 100 | 150 |
| 3 | 0 | 200 | 100 |
| 4 | -100 | 300 | 20 |
| 5 | 000 | 400 | 0 |

Table 3: Via-points for task II: S-shape motion

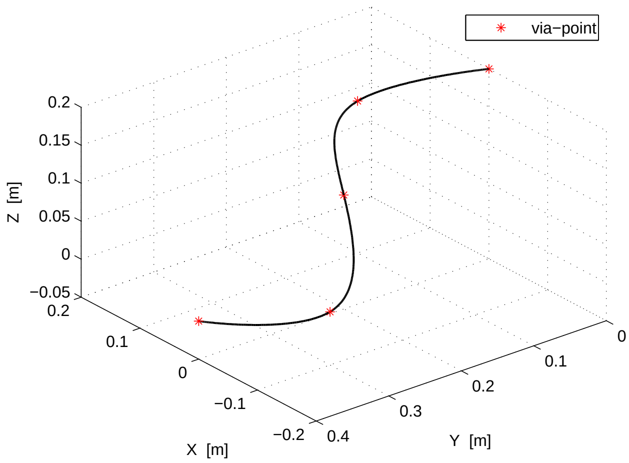


Figure 12: Task II: via-points and end-effector path in the operative space, 434 trajectory

Figs. 12,15 and 18 show the end-effector path associated with the optimal solution for each of the three additional tasks when using the 434 planning strategy, as well as the prescribed via-points.

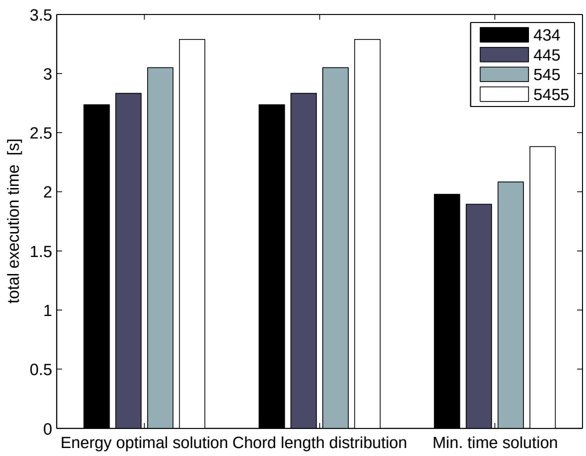


Figure 13: Total execution time for task II, with the four trajectories: comparison between energy-optimal solutions, chord-length time distribution and minimum time solutions

The effects of the application of the proposed energy optimization method are again compared with the results arising from a trajectory design based on a minim time criterion, and on a chord length distribution criterion, focusing on task II, III and IV.

The total execution time and the total energy consumption required when executing task II are shown in Fig. 13. According to such data, all the four primitives ensure that a chord-length distribution of the time intervals is compatible with the kinematic limits, so that no time scaling is needed to slow-down the speed of motion. On the average, the minimum time solution is roughly 1 s faster than the energy-optimal solution, but looking at Fig. 14 reveals that the increased speed comes with a sensible increase of the overall energy consumption, which ranges from 29 % to 56 %. Figures 13 and 14 show that, even if the total execution time is kept the same, the

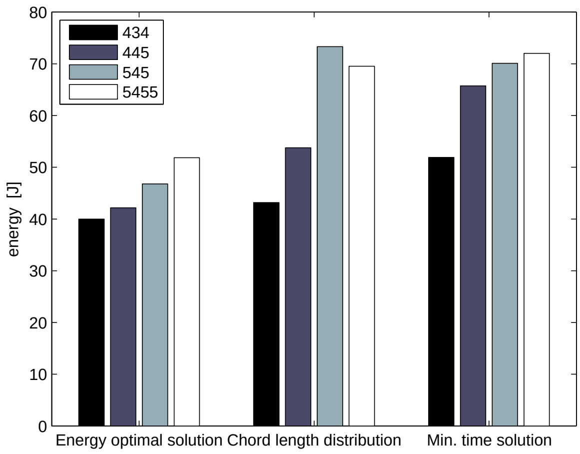


Figure 14: Energy consumption for task II, with the four trajectories: comparison between energy-optimal solutions, chord-length time distribution and minimum time solutions

choice of the distribution of the time intervals has a major effect on the energy consumption: for the task under consideration the use of a chord length distribution in lieau of an energy-optimal distribution requires an additional energetic cost that ranges from 8 % to 57 %.

| Via-point | X [mm] | Y [mm] | Z [mm] |
|---|---|---|---|
| 1 | 0 | 0 | 0 |
| 2 | 10 | 0 | 0 |
| 3 | 20 | 0 | 0 |
| 4 | 30 | 0 | 0 |
| 5 | 40 | 0 | 0 |
| 6 | 30 | 70.7 | 70.7 |
| 7 | 20 | 141.4 | 141.4 |
| 8 | 10 | 212.8 | 212.8 |
| 9 | 0 | 282.8 | 282.8 |
| 10 | 0 | 212.1 | 212.1 |
| 11 | 0 | 141.4 | 141.4 |
| 12 | 0 | 70.7 | 70.7 |
| 13 | 0 | 0 | 0 |

Table 4: Via-points for task III: triangular trajectory

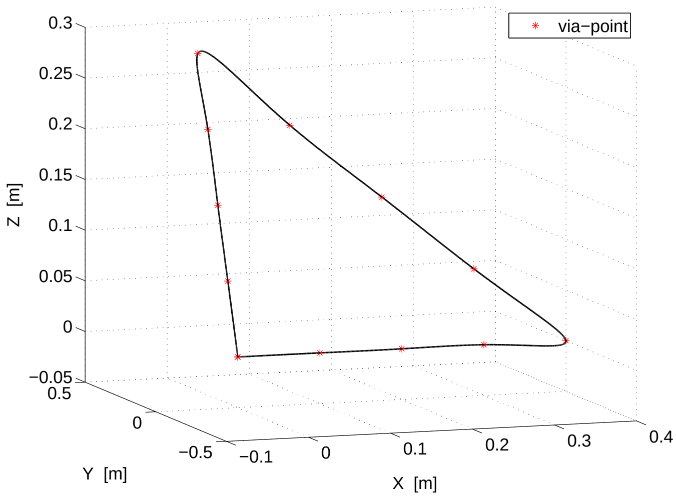


Figure 15: Task III: via-points and end-effector path in the operative space, 434 trajectory

Figure 16 and 17 highlight that the use of a chord length distribution is not a sensible choice for the timing of the trajectory for the 'triangular shape' task, given that it leads to notably high total execution time, as for the 434 and 445 motion primitives, and high energy consumption, as for the 545 and 5455 trajectories. An apparent proportionality can be detected when comparing the results of the application of the minimum time and of the minimum energy criteria: the fastest solution requires in the average roughly 60 % more energy but the total exectuion time is reduced, approximately, by one third.

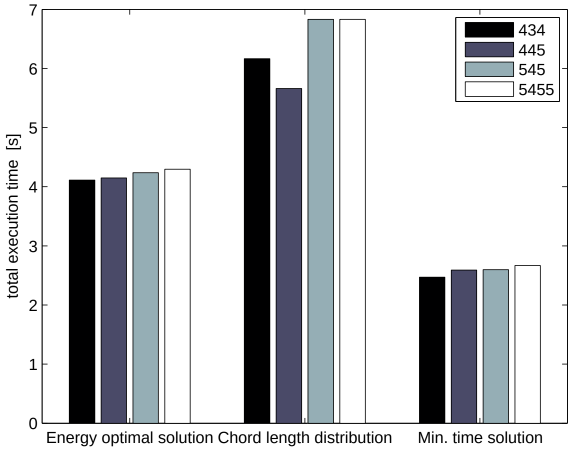


Figure 16: Total execution time for task III, with the four trajectories: comparison between energy-optimal solutions, chord-length time distribution and minimum time solutions

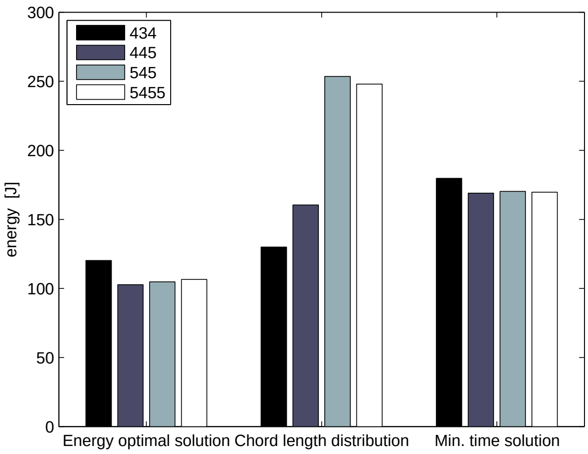


Figure 17: Energy consumption for task III, with the four trajectories: comparison between energy-optimal solutions, chord-length time distribution and minimum time solutions

This is a pre-print of an article published in The International Journal of Advanced Manufacturing Technology.
The final authenticated version is available online at: https://doi.org/10.1007/s00170-018-03234-4

| Via-point | X [mm] | Y [mm] | Z [mm] |
|---|---|---|---|
| 1 | 0 | 0 | 0 |
| 2 | 0 | 141.4 | 141.4 |
| 3 | 0 | 282.8 | 282.8 |
| 4 | 100 | 282.8 | 282.8 |
| 5 | 200 | 282.8 | 282.8 |
| 6 | 300 | 282.8 | 282.8 |
| 7 | 400 | 282.8 | 282.8 |
| 8 | 400 | 141.4 | 141.4 |
| 9 | 400 | 0 | 0 |
| 10 | 300 | 0 | 0 |
| 11 | 200 | 0 | 0 |
| 12 | 100 | 0 | 0 |
| 13 | 0 | 0 | 0 |

Table 5: Via-points for task IV: Square

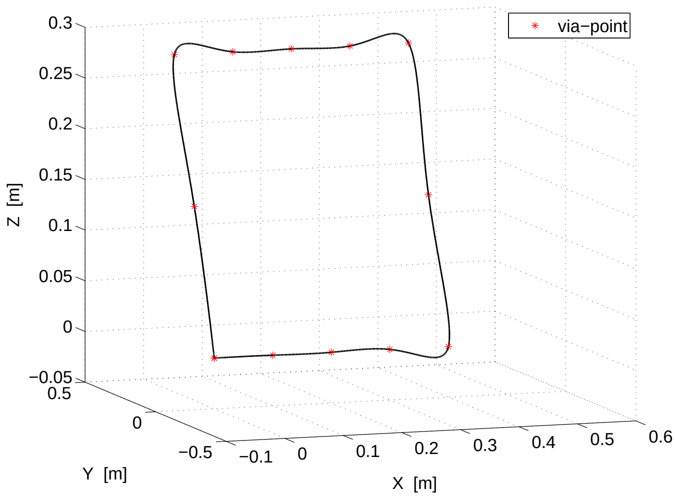


Figure 18: Task IV: via-points and end-effector path in the operative space, 434 trajectory

Figures 19 and 20 condensate the results of the application of the three motion design method to the test case IV. Fig. 19 highlights that application of a chord length distribution timing strategy results in very slow trajectories as the result of the time scaling required to ensure the respect of kinematic constraints. This time distribution is also quite energetically inefficient, provided that the associated energy costs are not very dissimilar to the one resulting from a minimum time criterion. On the average, the minimum time solution requires one third less time and 44 % more energy than the energy-optimal solution.

Overall, the data shows that the chord-length distribution is not a suggested choice when high performance is required, since it often leads to long execution times without trading off for a reduced energy consumption, given that often the trajectories are both slower than the energy-optimal ones and more energetically expensive than the minimum-time ones. In practical applications, in which a time-energy tradeoff might be favored, it might be suggested to use mixed cost optimization designs, such as a weighted time-energy criterion optimization, or to optimize the energy with a total execution time constraint.

This is a pre-print of an article published in The International Journal of Advanced Manufacturing Technology.
The final authenticated version is available online at: https://doi.org/10.1007/s00170-018-03234-4

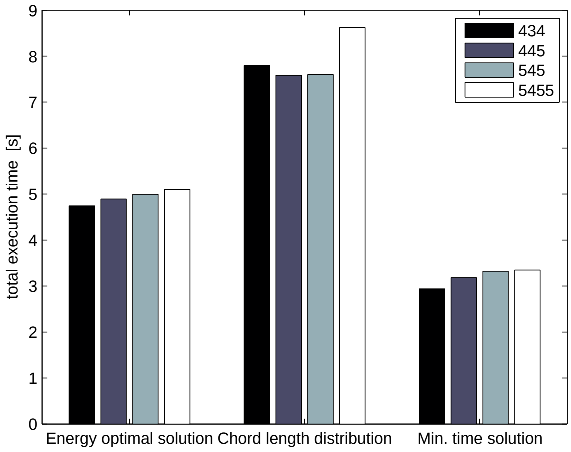


Figure 19: Total execution time for task IV, with the four trajectories: comparison between energy-optimal solutions, chord-length time distribution and minimum time solutions

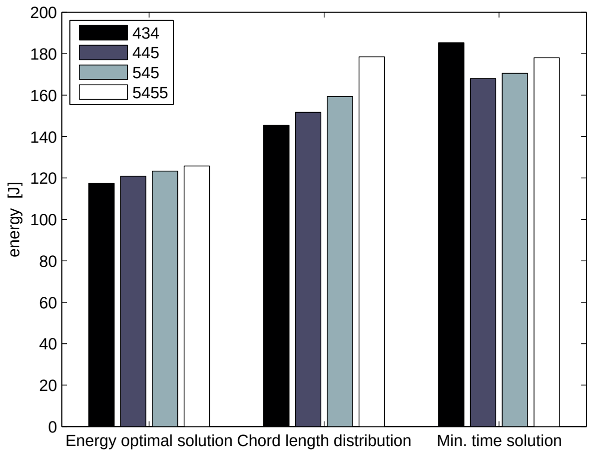


Figure 20: Total execution time for task IV, with the four trajectories: comparison between energy-optimal solutions, chord-length time distribution and minimum time solutions

This is a pre-print of an article published in The International Journal of Advanced Manufacturing Technology.
The final authenticated version is available online at: https://doi.org/10.1007/s00170-018-03234-4

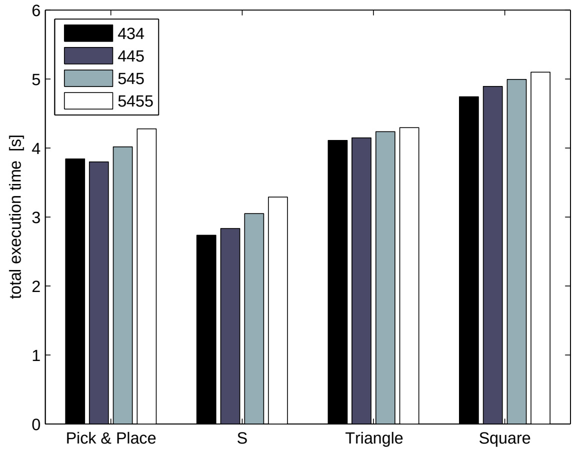


Figure 21: Tasks I-IV: comparison of total execution time, minimum energy criterion

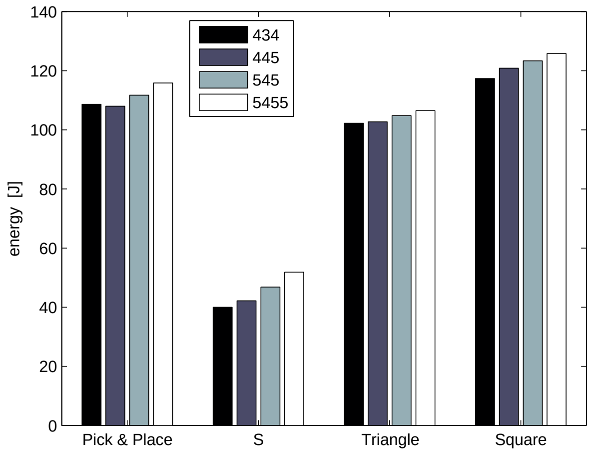


Figure 22: Tasks I-IV: comparison of energetic cost, minimum energy criterion

An overall comparison between the execution times and the energy costs resulting from the application of the energy-optimal criterion when reproducing all four tasks can be performed by analyzing the data presented in Fig. 21 and Fig. 22.

Such figures shows that the shorter execution times are, generally, the result of using lower degree primitives. In particular, the 434 trajectories ensures both minimum execution time and energy consumption for all the examined tasks, with the exception of the pick & place task, for which the 445 ensures a marginally better results.

The difference between the total energy consumption and the total execution time among the four solution in executing the same task are not negligible and therefore worth of investigation. The data collected in Figs. 21 and 22 show that the best choice in terms of motion primitive can achieve a speed-up up to 20.20 % and energy reduction up to 29.63 %. The results also highlights, for the robot and for the tasks under consideration, a general tradeoff between motion smoothness and energy consumption.

This is a pre-print of an article published in The International Journal of Advanced Manufacturing Technology.
The final authenticated version is available online at: https://doi.org/10.1007/s00170-018-03234-4

## 6.1 Motor power limitation

A meaningful extension of the optimization problem in Eq. 38 is the inclusion of additional constraints, since that formulation refers only to kinematic quantities. Additional constraints can be useful when it is needed to cope with other physical limitations of the manipulator.

One possible scenario that requires an extension of the aforementioned optimization framework is the limitation of the electric power at the motor drives. In particular, it might be convenient to constrain the the maximum values of the electric power which can flow from the drive to the motor or, when regeneration happens, in the opposite direction. In non-regenerative systems it might be needed also to account for the maximum power dissipation on the braking resistors [9].

The numerical solution to the optimization problem when augmented with electric power limitations requires to evaluate the extreme values of current in each $k$-th segment and for each joint of the robot for each iteration of the numerical solver. The most straightforward method to evaluate the extreme values of current is to evaluate the voltage-current product for a sufficiently large number of time samples in the range $[0, T_k]$, for each segment and each robot axis using Eqs. 1 and 2. Such a method has the disadvantage of requiring an unnecessary amount of computing resources, since it would be better to evaluate the magnitude of the electric power only where a local minimum or maximum might be located.

To detect where a minimum or a maximum value of the electric power can be located, a slight reformulation of Eqs. 20,21,28,35 is useful. In particular, the terms $W_{2,k}$ in Eq. 28 and $W_{3,k}$ in Eq. 35 can be merged into the single one:

$$W_{2,k} + W_{3,k} = T_c \left( 2\frac{R}{k_t^2} \left( J\ddot{q}_k(t) + T_{ext} + f_v \dot{q}_k(t) \right) + \frac{k_b}{k_t} \right) sgn\left( \dot{q}_k(t) \right) \tag{39}$$

Equation (39) takes a polynomial form, owing to the polynomial formulation adopted to describe joint speed $\dot{q}_k(t)$ and joint acceleration $\ddot{q}_k(t)$, that for the intermediate segments of a 434 trajectory can be written as:

$$W_{2,k} + W_{3,k} = \pm \sum_{i=0}^{2} w_{k,i}^{23} t^i \tag{40}$$

in which the term $sgn(\dot{q}(t))$ is replaced by the $'\pm'$ symbol. By including the electric power term $W_{1,k}$ too, according to Eqs. 20, 21 and 40, the total electric power drawn by one motor during the $k$-th segment of the trajectory is:

$$W_k(t) = \sum_{i=0}^{4} w_{i,k} t^i \pm \sum_{i=0}^{2} w_{i,k}^{23} t^i \tag{41}$$

The latter is equivalent to two fourth-degree polynomial equations, one obtained with the 'plus' and the other with the 'minus' according to the sign of the joint speed at time $t$. The possible locations of the maxima and minima of the power $W_k(t)$ are easily found by identifying the zeros of its time derivative $\dot{W}_k$, which are readily available using closed-form formulas for lower-degree motion primitives or the aforementioned matrix companion method. Once the time instant for each possible maximum or minimum is found, the actual sign of the joint speed can be evaluated and the corresponding numerical value of $W_k(t)$ can therefore be discarded or kept for the computation of the extremal values of the electric power.

Extensive tests have shown that the suggested method of computing the extremal values of the current has a very limited impact on the required computing effort, given the limited amount of additional computation introduced by the proposed method.

The effectiveness of the method is shown in Fig. 23, which reports the electric power absorbed by each motor for the pick & place trajectory and the 434 planning method. The largest amount of electric is delivered to the Z axis actuator, which has to counteract the gravity force while producing the initial 'lifting' motion. The power limit is set, for all three motors, to $\pm 120$ W. The electric power profiles show that the electric power that is provided by the each drive circuit

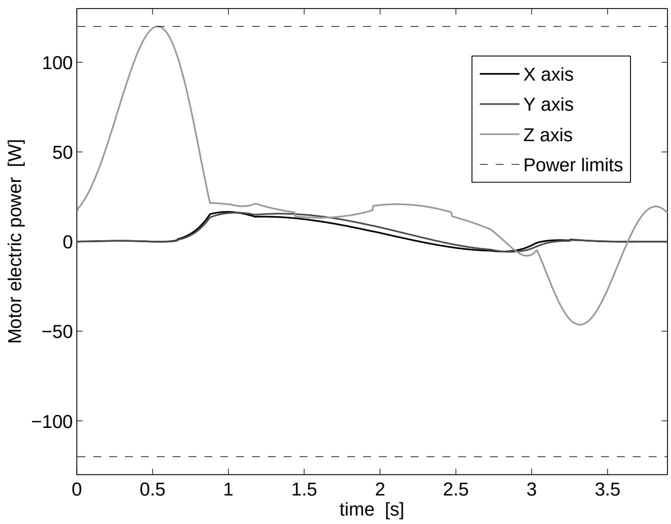


Figure 23: Pick & place task: motor power with bounded motor electric power

to the corresponding motor is precisely limited to the prescribed bound. The results take into consideration a symmetrical power limitation to each individual motor, but the same method can be, as a matter of example, easily extended to take into account different or additional constraints, such as bounds on the total electric power delivered to the whole robot or other generic bounds that might be non-symmetric.

# 7 Conclusions

In this work, a novel trajectory planning algorithm for industrial robots is proposed, aimed at minimizing the energy consumption of tasks defined as a set of via-points. The method can take into consideration constraints on speed, acceleration and jerk for each joint of the robot, as well as limits on the electric power capabilities of the electric drives. The method is suitable for single and multiple joint robots with uncoupled dynamics, such as gantry cranes or Cartesian robots, driven by regenerative drives. An optimization problem is defined and solved by computing the closed-form solutions of electric energy and power for the 434, 445, 545 and 5455 trajectories. The availability of a closed-form analytic expression of energy consumption allows to solve the optimization problem with algebraic equations without the need to integrate the differential dynamic equations of motion of the robot, thus ensuring maximum computational efficiency. The results indicate that, for the benchmark robot and the tasks under consideration, the use of lower-degree motion profiles are generally the best choice in term of energy saving. In some cases however a smoother trajectory can be preferred to limit the peak values of the joint acceleration, as detected for the pick & place test-case analyzed in this work.

# References

[1] D. Helm, "The european framework for energy and climate policies," *Energy Policy*, vol. 64, pp. 29–35, 2014.

[2] A. Fysikopoulos, G. Pastras, T. Alexopoulos, and G. Chryssolouris, "On a generalized approach to manufacturing energy efficiency," *The International Journal of Advanced Manufacturing Technology*, vol. 73, no. 9-12, pp. 1437–1452, 2014.

[3] M. Brossog, M. Bornschlegl, J. Franke *et al.*, "Reducing the energy consumption of industrial

robots in manufacturing systems," *The International Journal of Advanced Manufacturing Technology*, vol. 78, no. 5-8, pp. 1315–1328, 2015.

[4] T. Fleiter and W. Eichhammer, "Energy efficiency in electric motor systems: Technology, saving potentials and policy options for developing countries," *Development Policy, Statistics And Research Branch Working Paper*, vol. 11, 2011.

[5] T. Peng and X. Xu, "Energy-efficient machining systems: a critical review," *The International Journal of Advanced Manufacturing Technology*, vol. 72, no. 9-12, pp. 1389–1406, 2014.

[6] Z. Yingjie, "Energy efficiency techniques in machining process: a review," *The International Journal of Advanced Manufacturing Technology*, vol. 71, no. 5-8, pp. 1123–1132, 2014.

[7] T. Lerher, M. Edl, and B. Rosi, "Energy efficiency model for the mini-load automated storage and retrieval systems," *The International Journal of Advanced Manufacturing Technology*, vol. 70, no. 1-4, pp. 97–115, 2014.

[8] D. Meike and L. Ribickis, "Analysis of the energy efficient usage methods of medium and high payload industrial robots in the automobile industry," in *10th International Symposium Topical Problems in the Field of Electrical and Power Engineering Pärnu, Estonia*, 2011.

[9] D. Meike, A. Senfelds, and L. Ribickis, "Power converter for DC bus sharing to increase the energy efficiency in drive systems," in *Industrial Electronics Society, IECON 2013-39th Annual Conference of the IEEE*. IEEE, 2013, pp. 7199–7204.

[10] D. Meike and L. Ribickis, "Energy efficient use of robotics in the automobile industry," in *2011 15th International Conference on Advanced Robotics (ICAR)*, June 2011, pp. 507–511.

[11] G. Carabin, E. Wehrle, and R. Vidoni, "A review on energy-saving optimization methods for robotic and automatic systems," *Robotics*, vol. 6, no. 4, p. 39, 2017.

[12] M. Hazan, L. Embon, and R. Madvil, "Method and apparatus for saving energy and reducing cycle time by using optimal robotic joint configurations," Mar. 29 2016, US Patent 9,298,863.

[13] M. Frische and F. Jungnickel, "Reducing energy consumption of industrial robots by using new methods for motion path programming," May 16 2017, US Patent 9,649,765.

[14] E.-C. Corporation, *DC Motors, Speed controls, servo systems: An engineering handbook*. Pergamon Press.

[15] P. M. Ho, N. Uchiyama, S. Sano, K. Sawada, A. Kato, and T. Yonezawa, "Simple motion trajectory generation for energy saving of industrial machines," in *System Integration (SII), 2012 IEEE/SICE International Symposium on*. IEEE, 2012, pp. 476–480.

[16] P. Boscariol, G. Carabin, A. Gasparetto, N. Lever, and R. Vidoni, "Energy-efficient point-to-point trajectory generation for industrial robotic machines," in *proceedings of the 2015 ECCOMAS Thematic Conference on Multibody System Dynamics*, 2015, pp. 1425–1433.

[17] D. Richiedei and A. Trevisani, "Analytical computation of the energy-efficient optimal planning in rest-to-rest motion of constant inertia systems," *Mechatronics*, vol. 39, pp. 147–159, 2016.

[18] K. Inoue, K. Ogata, and T. Kato, "An efficient power regeneration and drive method of an induction motor by means of an optimal torque derived by variational method," *IEEJ Transactions on Industry Applications*, vol. 128, pp. 1098–1105, 2008.

[19] K. Inoue, Y. Asano, K. Kotera, and T. Kato, "Optimal energy saving trajectories of induction motor with suppression of sudden acceleration and deceleration," in *Energy Conversion Congress and Exposition (ECCE), 2014 IEEE*. IEEE, 2014, pp. 3219–3223.

[20] J. T. Betts, "Survey of numerical methods for trajectory optimization," *Journal of Guidance control and dynamics*, vol. 21, no. 2, pp. 193–207, 1998.

[21] C. Hansen, J. Kotlarski, and T. Ortmaier, "Experimental validation of advanced minimum energy robot trajectory optimization," in *Advanced Robotics (ICAR), 2013 16th International Conference on.* IEEE, 2013, pp. 1–8.

[22] C. Hansen, K. Eggers, J. Kotlarski, and T. Ortmaier, "Comparative evaluation of energy storage application in multi-axis servo systems," in *Proceedings of the 14th IFToMM World Congress, Taipei, Taiwan*, 2015.

[23] G. Berselli, F. Balugani, M. Pellicciari, and M. Gadaleta, "Energy-optimal motions for servo-systems: A comparison of spline interpolants and performance indexes using a CAD-based approach," *Robotics and Computer-Integrated Manufacturing*, vol. 40, pp. 55–65, 2016.

[24] M. Pellicciari, G. Berselli, and F. Balugani, "On designing optimal trajectories for servo-actuated mechanisms: Detailed virtual prototyping and experimental evaluation," *IEEE/ASME Transactions on Mechatronics*, vol. 20, no. 5, pp. 2039–2052, 2015.

[25] C. Hansen, J. Öltjen, D. Meike, and T. Ortmaier, "Enhanced approach for energy-efficient trajectory generation of industrial robots," in *Automation Science and Engineering (CASE), 2012 IEEE International Conference on.* IEEE, 2012, pp. 1–7.

[26] O. Al-Naseem, R. W. Erickson, and P. Carlin, "Prediction of switching loss variations by averaged switch modeling," in *Applied Power Electronics Conference and Exposition, 2000. APEC 2000. Fifteenth Annual IEEE*, vol. 1. IEEE, 2000, pp. 242–248.

[27] J. Park, "Motion profile planning of repetitive point-to-point control for maximum energy conversion efficiency under acceleration conditions," *Mechatronics*, vol. 6, no. 6, pp. 649–663, 1996.

[28] Z. Yu, C. Han, and M. Haihua, "A novel approach of tuning trapezoidal velocity profile for energy saving in servomotor systems," in *Control Conference (CCC), 2015 34th Chinese.* IEEE, 2015, pp. 4412–4417.

[29] T. Verstraten, R. Furnémont, G. Mathijssen, B. Vanderborght, and D. Lefeber, "Energy consumption of geared dc motors in dynamic applications: Comparing modeling approaches," *IEEE Robotics and Automation Letters*, vol. 1, no. 1, pp. 524–530, 2016.

[30] K. Inoue, K. Kotera, and T. Kato, "Optimal torque trajectories minimizing loss of induction motor under given condition of rotational angle," in *Energy Conversion Congress and Exposition (ECCE), 2011 IEEE.* IEEE, 2011, pp. 1734–1738.

[31] C. Cavallaro, A. O. Di Tommaso, R. Miceli, A. Raciti, G. R. Galluzzo, and M. Trapanese, "Efficiency enhancement of permanent-magnet synchronous motor drives by online loss minimization approaches," *IEEE Transactions on Industrial Electronics*, vol. 52, no. 4, pp. 1153–1160, 2005.

[32] S. Gale, A. A. Eielsen, and J. T. Gravdahl, "Modelling and simulation of a flywheel based energy storage system for an industrial manipulator," in *Industrial Technology (ICIT), 2015 IEEE International Conference on.* IEEE, 2015, pp. 332–337.

[33] L. Biagiotti and C. Melchiorri, *Trajectory planning for automatic machines and robots.* Springer Science & Business Media, 2008.

[34] H. Liu, X. Lai, and W. Wu, "Time-optimal and jerk-continuous trajectory planning for robot manipulators with kinematic constraints," *Robotics and Computer-Integrated Manufacturing*, vol. 29, no. 2, pp. 309–317, 2013.

This is a pre-print of an article published in The International Journal of Advanced Manufacturing Technology.
The final authenticated version is available online at: https://doi.org/10.1007/s00170-018-03234-4

[35] C. Cook and C. Ho, *The application of spline functions to trajectory generation for computer-controlled manipulators*. Springer, 1984.

[36] K. Petrinec and Z. Kovacic, "Trajectory planning algorithm based on the continuity of jerk," in *Control & Automation, 2007. MED'07. Mediterranean Conference on*. IEEE, 2007, pp. 1–5.

[37] P. Boscariol, A. Gasparetto, and R. Vidoni, "Planning continuous-jerk trajectories for industrial manipulators," in *ASME 2012 11th Biennial Conference on Engineering Systems Design and Analysis*. American Society of Mechanical Engineers, 2012, pp. 127–136.

[38] A. Edelman and H. Murakami, "Polynomial roots from companion matrix eigenvalues," *Mathematics of Computation*, vol. 64, no. 210, pp. 763–776, 1995.

# Appendix: Polynomial coefficients of electric power

## First segment of the '434' trajectory: polynomial coefficients $w^{434}_{i,1}$

$$w^{434}_{6,1} = \frac{16{b_4}^2 f\left(Rf + k_b k_t\right)}{{k_t}^2}$$

$$w^{434}_{5,1} = \frac{24 b_4 k_b \left(2Jb_4 + b_3 f\right)}{k_t} + \frac{24 R b_4 f \left(4Jb_4 + b_3 f\right)}{{k_t}^2}$$

$$w^{434}_{4,1} = \frac{3R\left(48J^2{b_4}^2 + 40Jb_3 b_4 f + 3{b_3}^2 f^2\right)}{{k_t}^2} + \frac{3 b_3 k_b \left(20Jb_4 + 3b_3 f\right)}{k_t}$$

$$w^{434}_{3,1} = \frac{2k_b\left(9J{b_3}^2 + 2T_{ext} b_4\right)}{k_t} + \frac{4R\left(b_4 J^2 b_3 36 + fJ{b_3}^2 9 + 2T_{ext} b_4 f\right)}{{k_t}^2}$$

$$w^{434}_{2,1} = \frac{6R\left(6J^2{b_3}^2 + T_{ext} b_4 J 4 + T_{ext} f b_3\right)}{{k_t}^2} + \frac{3T_{ext} b_3 k_b}{k_t}$$

$$w^{434}_{1,1} = \frac{12JRT_{ext} b_3}{{k_t}^2}$$

$$w^{434}_{0,1} = \frac{R\left({T_c}^2 + {T_{ext}}^2\right)}{{k_t}^2}$$

## Last segment of the '434' trajectory: polynomial coefficients $w^{434}_{i,N-1}$:

$$w^{434}_{6,N-1} = \frac{16{b_5}^2 f_v \left(Rf_v + k_b k_t\right)}{{k_t}^2}$$

$$w^{434}_{5,N-1} = \frac{24 b_5 k_b \left(2Jb_5 + b_4 f\right)}{k_t} + \frac{24 R b_5 f_v \left(4Jb_5 + b_4 f\right)}{{k_t}^2}$$

$$w^{434}_{4,N-1} = \frac{R\left(144J^2{b_5}^2 + 120Jb_4 b_5 f_v + 9{b_4}^2 f^2 + 16 b_3 b_5 f^2\right)}{{k_t}^2} + \frac{k_b\left(f_v {b_4}^2 9 + Jb_5 b_4 60 + 16 b_3 b_5 f\right)}{k_t}$$

$$w^{434}_{3,N-1} = \frac{4R\left(b_5 J^2 b_4 36 + 9J{b_4}^2 f_v + b_3 b_5 J f_v 16 + 3b_3 b_4 f^2 + 2b_2 b_5 f^2 + 2T_e b_5 f\right)}{{k_t}^2} + \frac{2k_b\left(9J{b_4}^2 + b_3 f_v b_4 6 + 2T_e b_5 + 16Jb_3 b_5 + 4b_2 b_5 f\right)}{k_t}$$

$$w^{434}_{2,N-1} = \frac{2R\left(b_5 J^2 b_3 24 + 18J^2{b_4}^2 + 18Jb_3 b_4 f_v + b_2 b_5 J f_v 12 + T_e b_5 J 12 + 2{b_3}^2 f^2 + 3b_2 b_4 f^2 + 3T_e b_4 f\right)}{{k_t}^2} + \frac{k_b\left(f_v {b_3}^2 4 + Jb_4 b_3 18 + 3T_e b_4 + 12Jb_2 b_5 + 6b_2 b_4 f\right)}{k_t}$$

$$w^{434}_{1,N-1} = \frac{2k_b\left(T_e b_3 + 2J{b_3}^2 + 3Jb_2 b_4 + 2b_2 b_3 f\right)}{k_t} + \frac{4R\left(3Jb_4 + b_3 f\right)\left(T_e + 2Jb_3 + b_2 f\right)}{{k_t}^2}$$

$$w^{434}_{0,N-1} = \frac{R\left(4J^2{b_3}^2 + 4JT_e b_3 + 4Jb_2 b_3 f_v + {T_c}^2 + {T_e}^2 + 2T_e b_2 f_v + {b_2}^2 f^2\right)}{{k_t}^2} + \frac{b_2 k_b\left(T_e + 2Jb_3 + b_2 f\right)}{k_t}$$

The coefficients $w^{434}_{i,N-1}$ can be used also for a generic fourth-degree segment, as in the 445, 545 or 5455 trajectory.

This is a pre-print of an article published in The International Journal of Advanced Manufacturing Technology.
The final authenticated version is available online at: https://doi.org/10.1007/s00170-018-03234-4

# Fifth-degree segments:

$$w_{8,k}^{5^{th}} = \frac{25\, b_6{}^2\, f\ (R\, f_v + k_b\, k_t)}{k_t{}^2}$$

$$w_{7,k}^{5^{th}} = \frac{20 b_6 k_b\, (5 J b_6 + 2 b_5 f)}{k_t} + \frac{40 R b_6 f_v\, (5 J b_6 + b_5 f)}{k_t{}^2}$$

$$w_{6,k}^{5^{th}} = \frac{2R\left(200 J^2 b_6{}^2 + 140 J b_5 b_6 f_v + 8 b_5{}^2 f^2 + 15 b_4 b_6 f^2\right)}{k_t{}^2} + \frac{2k_b\left(f_v b_5{}^2 8 + J b_6 b_5 70 + 15 b_4 b_6 f\right)}{k_t}$$

$$w_{5,k}^{5^{th}} = \frac{4R\left(b_6 J^2 b_5 120 + 24 J b_5{}^2 f_v + b_4 b_6 J f_v 45 + 6 b_4 b_5 f^2 + 5 b_3 b_6 f^2\right)}{k_t{}^2} + \frac{2k_b\left(24 J b_5{}^2 + b_4 f_v b_5 12 + 45 J b_4 b_6 + 10 b_3 b_6 f\right)}{k_t}$$

$$w_{4,k}^{5^{th}} = \frac{R\left(b_6 J^2 b_4 240 + 144 J^2 b_5{}^2 + 120 J b_4 b_5 f_v + b_3 b_6 J f_v 100 + 9 b_4{}^2 f^2 + 16 b_3 b_5 f^2 + 10 b_2 b_6 f^2 + 10 T_{ext} b_6 f\right)}{k_t{}^2} + \frac{k_b\left(f_v b_4{}^2 9 + J b_5 b_4 60 + 5 T_{ext} b_6 + 50 J b_3 b_6 + 10 b_2 b_6 f_v + 16 b_3 b_5 f\right)}{k_t}$$

$$w_{3,k}^{5^{th}} = \frac{2k_b\left(9 J b_4{}^2 + b_3 f_v b_4 6 + 2 T_{ext} b_5 + 10 J b_2 b_6 + 16 J b_3 b_5 + 4 b_2 b_5 f\right)}{k_t} + \frac{4R\left(10 J T_{ext} b_6 + 2 T_{ext} b_5 f_v + 20 J^2 b_3 b_6 + 36 J^2 b_4 b_5 + 9 J b_4{}^2 f_v + 2 b_2 b_5 f^2 + 3 b_3 b_4 f^2 + 10 J b_2 b_6 f_v + 16 J b_3 b_5 f\right)}{k_t{}^2}$$

$$w_{2,k}^{5^{th}} = \frac{2R\left(b_5 J^2 b_3 24 + 18 J^2 b_4{}^2 + 18 J b_3 b_4 f_v + b_2 b_5 J f_v 12 + T_{ext} b_5 J 12 + 2 b_3{}^2 f^2 + 3 b_2 b_4 f^2 + 3 T_{ext} b_4 f\right)}{k_t{}^2} + \frac{k_b\left(f_v b_3{}^2 4 + J b_4 b_3 18 + 3 T_{ext} b_4 + 12 J b_2 b_5 + 6 b_2 b_4 f\right)}{k_t}$$

$$w_{1,k}^{5^{th}} = \frac{2k_b\left(T_{ext} b_3 + 2 J b_3{}^2 + 3 J b_2 b_4 + 2 b_2 b_3 f\right)}{k_t} + \frac{4R\, (3 J b_4 + b_3 f)\, (T_{ext} + 2 J b_3 + b_2 f)}{k_t{}^2}$$

$$w_{0,k}^{5^{th}} = \frac{R\left(4 J^2 b_3{}^2 + 4 J T_{ext} b_3 + 4 J b_2 b_3 f_v + T_c{}^2 + T_{ext}{}^2 + 2 T_{ext} b_2 f_v + b_2{}^2 f^2\right)}{k_t{}^2} + \frac{b_2 k_b\, (T_{ext} + 2 J b_3 + b_2 f)}{k_t}$$

This is a pre-print of an article published in The International Journal of Advanced Manufacturing Technology.
The final authenticated version is available online at: https://doi.org/10.1007/s00170-018-03234-4